Applied Catalysis B: Environmental 92 (2009) 234–239

Contents lists available at ScienceDirect

Applied Catalysis B: Environmental

journal homepage: www.elsevier.com/locate/apcatb

Review

High temperature $SrCe_{0.9}Eu_{0.1}O_{3-\delta}$ proton conducting membrane reactor for H_2 production using the water–gas shift reaction

Jianlin Li, Heesung Yoon, Tak-Keun Oh, Eric D. Wachsman *

Florida Institute for Sustainable Energy, University of Florida, Gainesville, FL 32611, USA

ARTICLE INFO

Article history:
Received 1 April 2009
Received in revised form 4 August 2009
Accepted 17 August 2009
Available online 25 August 2009

Keywords:
Water–gas shift reaction
Proton conducting membrane
Hydrogen
Permeation
$SrCe_{0.9}Eu_{0.1}O_{3-\delta}$

ABSTRACT

The water–gas shift (WGS) reaction is used to shift the CO/H_2 ratio prior to Fischer–Tropsch synthesis and/or to increase H_2 yield. A WGS membrane reactor was developed using a mixed protonic–electronic conducting $SrCe_{0.9}Eu_{0.1}O_{3-\delta}$ membrane coated on a Ni–$SrCeO_{3-\delta}$ support. The membrane reactor overcomes the thermodynamic equilibrium limitations. A 46% increase in CO conversion and total H_2 yield was achieved at 900 °C under 3% CO and 6% H_2O, resulting in a 92% single pass H_2 production yield and 32% single pass yield of pure permeated H_2.

Contents

1. Introduction . . . 234
2. Experimental . . . 235
3. Results and discussion . . . 235
   3.1. Thermodynamic calculation . . . 235
   3.2. Experimental conversion . . . 236
   3.3. H_2 production . . . 238
4. Conclusions . . . 239
   Acknowledgements . . . 239
   References . . . 239

1. Introduction

The water–gas shift (WGS) reaction converts CO into CO_2 and provides additional H_2 via the following:

$$H_2O + CO \leftrightarrow H_2 + CO_2 \qquad \Delta H^\circ = -40.6\,kJ\,mol^{-1} \qquad (1)$$

It is often used in conjunction with steam reforming of methane or other hydrocarbons and is of central importance in the industrial production of H_2, ammonia, and other bulk chemical utilizing syngas [1].

The WGS reaction is typically a two-stage shift process, a high-temperature WGS and a low-temperature WGS, with each process employing separate catalysts [2,3]. New ceramic membranes have potential for cost reduction of synthesis gas production by 30–50% [4] and provide one solution to incorporate the WGS reaction and H_2 separation into one unit. Selective continuous removal of H_2 will drive the equilibrium of the shift reaction forward. As a result, the requirement to use a two-stage shift reaction and a cooling step can be eliminated and the WGS reaction may be carried out at higher temperatures [5]. This would allow the WGS reaction to be operated at a low H_2O/CO ratio without the thermodynamic constraint [6–8].

* Corresponding author at: Dept. of Materials Science and Engineering, University of Maryland, College Park, MD 20742-2115, USA. Tel.: +1 301 405 8193; fax: +1 301 314 2029.
E-mail address: ewach@umd.edu (E.D. Wachsman).

0926-3373/$ – see front matter © 2009 Elsevier B.V. All rights reserved.
doi:10.1016/j.apcatb.2009.08.015

High-temperature proton conductors such as $SrCeO_{3-\delta}$ would be well-suited for the H_2 separation step based on temperature considerations [5] if they had sufficient electronic conductivity to match their protonic conductivity. Several aliovalent ions (Y, Yb, Tb, Sm, Eu, Tm, etc.) have been used to partially substitute Ce to increase the electronic conductivity of $SrCeO_{3-\delta}$ [9–18]. Their protonic conductivities in hydrogen atmosphere are of the order of 10^{-2}–10^{-3} S cm^{-1} at 1000–600 °C [9]. The total conductivity of $SrCe_{0.95}Tm_{0.05}O_{3-\delta}$, $SrCe_{0.95}Tb_{0.05}O_{3-\delta}$, $SrCe_{0.95}Yb_{0.05}O_{3-\delta}$ and $SrCe_{0.9}Eu_{0.1}O_{3-\delta}$ is 0.06 [18], 0.07 [19], 0.12 [20] and 0.14 S/cm [13] at 900 °C, respectively. The activation energy is 0.49, 0.53, 0.77 and 0.67 eV, respectively. Generally, the activation enthalpies for the mobility of proton and electrons in perovskite-type oxides are 0.4–0.6 and 1 eV, respectively [21]. Therefore, higher activation energy indicates higher percentage of electronic conductivity in the total conductivity, and the electronic conductivity of $SrCeO_{3-\delta}$ is significantly improved by Eu doping. As a result, Eu doped $SrCeO_{3-\delta}$ is promising material for H_2 permeation. We previously reported the effect of dopant concentration in $SrCe_{1-x}Eu_xO_{3-\delta}$ ($0.05 \leq x \leq 0.2$) on ambipolar conductivity [22] and demonstrated that the maximum ambipolar conductivity increases with temperature and Eu dopant concentration. However, we also found that Eu dopant concentrations higher than 10 mol% result in mechanical instability. Therefore, $SrCe_{0.9}Eu_{0.1}O_{3-\delta}$ was used as the membrane material in this work. We have separately measured conductivity [22] and H_2 permeation [23] of the membrane and the conductivity is sufficient without Ni. Based on our previous experience, we fabricated a supported thin film membrane to increase H_2 permeation and NiO–$SrCeO_{3-\delta}$ was used to fabricate the support structure to maintain mechanical integrity. Eu was eliminated from the support composition since electronic conduction is not functionally necessary for the support. NiO was used to create porosity, by reduction to Ni when the membrane was subsequently exposed to H_2, and subsequent use of Ni as WGS catalyst. It is noted that no significant Ni was detected in the membrane itself after experiment by EDX indicating Ni does not contribute to the electronic conductivity of the membrane.

The thermodynamic equilibrium of the WGS reaction with H_2O/CO ratios of 1:1 and 2:1 was calculated. For the WGS reaction, carbon formation is detrimental as it causes catalyst deactivation. Appropriate operating temperature region without carbon formation for each H_2O/CO ratio was addressed. A WGS membrane reactor was developed using a $SrCe_{0.9}Eu_{0.1}O_{3-\delta}$ tubular membrane to incorporate the WGS reaction and H_2 separation into one unit. The improvement of CO conversion and H_2 production with the H_2 membrane reactor is discussed.

2. Experimental

Polycrystalline $SrCeO_{3-\delta}$ and $SrCe_{0.9}Eu_{0.1}O_{3-\delta}$ powders were prepared by conventional solid-state reaction by mixing stoichiometric amounts of $SrCO_3$ (99.9%, Alfa-Aesar), CeO_2 (99.9%, Alfa-Aesar) and Eu_2O_3 (99.9%, Alfa-Aesar) powders, followed by ball milling and calcining at 1300 °C. A NiO–$SrCeO_{3-\delta}$ tubular support was fabricated using tape-casting (Pro-Cast) followed by a rolling process. The tubular support was sealed at one end and pre-sintered. $SrCe_{0.9}Eu_{0.1}O_{3-\delta}$ was coated on the inner side of the pre-sintered support. The tubular membranes were finally sintered at 1450 °C. The sintering process was carried out in air atmosphere. A detailed preparation process has been discussed in our previous work [24].

The membrane tube was about 17 cm long and 0.48 cm in diameter (Fig. 1a). An SEM image shows the membrane is dense and ~23 μm thick on a porous support (Fig. 1b). A thermal insulator was applied to the bottom of the membrane tube, forming an insulating region to drop the temperature and allow O-ring sealing of the tube [23]. The area of the membrane above the insulator zone is considered the active area and is about 12 cm^2. The WGS reaction was carried out from 600 to 900 °C under 3% CO + 3% H_2O and 3% CO + 6% H_2O (total flow rate of 20 sccm balanced by Ar). Gas flow rates were controlled by mass flow controllers.

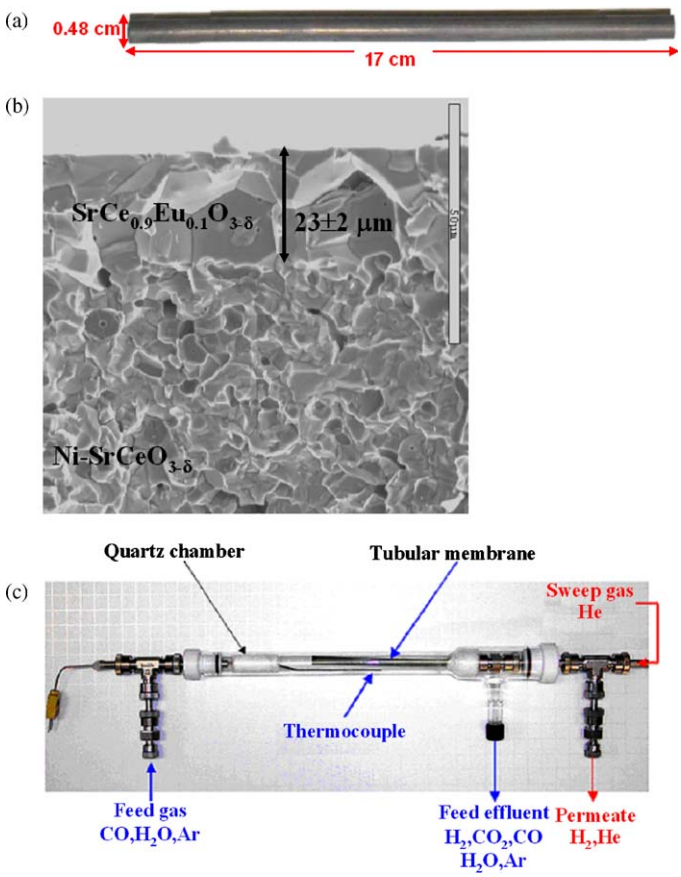

Fig. 1. (a) Membrane tube, (b) SEM image of sintered membrane cross section and (c) photo of the WGS reactor showing gas flow

Fig. 1c shows a photo of the experimental setup. A thermo couple was placed axially at the middle of the membrane to control temperature. Argon was used as tracer to detect leakage and there was no leakage detected in this experiment. The reactants, CO and H_2O, were flowed into the quartz chamber and exposed to the Ni catalyst on the outside of the membrane tube. The feed side effluents were analyzed by gas chromatography (Varian CP 4900). Helium was used as a sweep gas on the inner side of the membrane. The permeated H_2 together with Ar (leakage) were analyzed by a mass spectrometer (Q100MS Dycor Quadlink). The total pressure of the sweep gas and feed gas is 1 atm. A typical H_2 partial pressure difference over the membrane is about 0.01 atm in this work.

3. Results and discussion

3.1. Thermodynamic calculation

The thermodynamic equilibrium conditions of the WGS reaction were calculated using Thermocalc software [25] with a total pressure of 1 atm. Fig. 2(a) and (b) shows the temperature dependence on species mole fraction with feed H_2O/CO ratios of 1:1 and 2:1, respectively. The mole fractions of the reactants, CO and H_2O, increase with increasing temperature, which is attributed to the exothermic nature of the WGS reaction. Thus thermo-

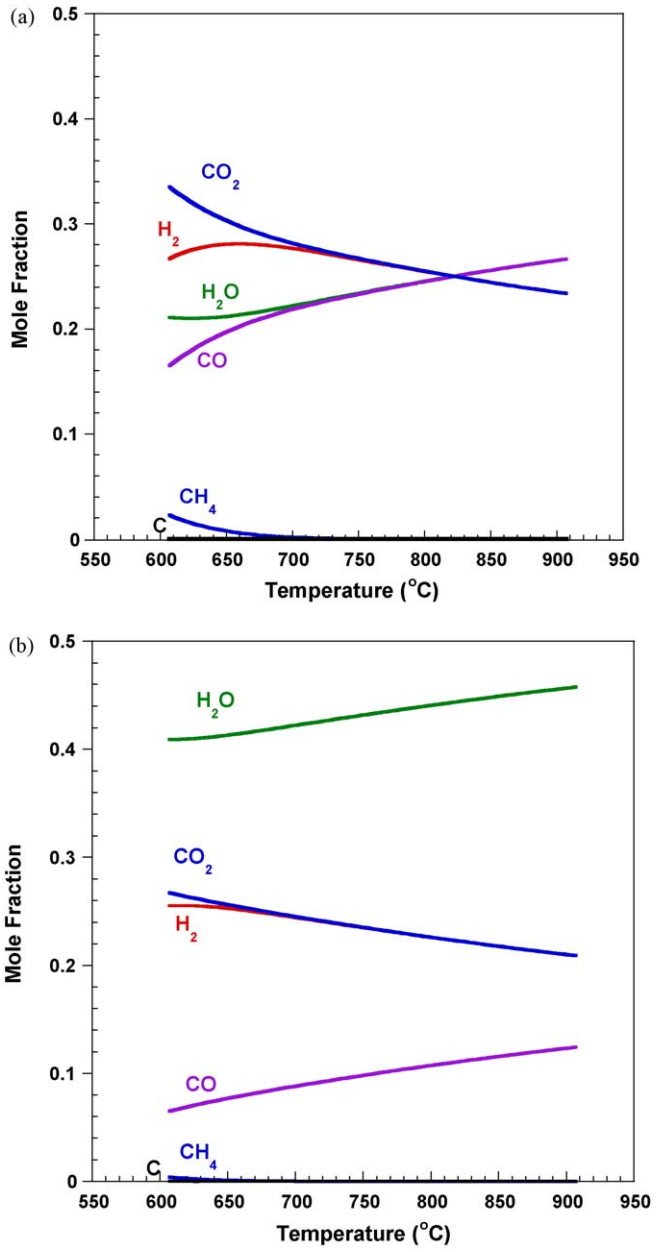

Fig. 2. Thermodynamic equilibrium of WGS (a) $H_2O/CO = 1:1$ and (b) $H_2O/CO = 2:1$.

dynamic equilibrium moves to the reactant side at elevated temperature.

Achieving a carbon deposition free operating temperature region is very important for the WGS reaction since carbon formation may block the pores of the porous support and lead to catalyst deactivation as well as cracking of the membrane. Thermodynamic equilibrium results show that carbon formation is in general favored at low temperature and low H_2O/CO ratio. When the H_2O/CO equals one, carbon will not form at temperatures higher than 590 °C. This shifts to 550 °C for a H_2O/CO ratio of two. This is in agreement with the results by Xue et al. [26]. They reported the risk of carbon formation due to side reactions increased as the H_2O/CO ratio decreased. The formation of carbon with a H_2O/CO ratio of 1 was thermodynamically favorable over the entire temperature range examined (up to 500 °C). However, a carbon-free operation condition was achieved at temperatures higher than 230 °C with a H_2O/CO ratio of 3.

Low temperatures also favor CH_4 and H_2O formation, which is clearly shown in Fig. 2(a). If no side reactions are considered, the mole fractions of CO and H_2O are equal to each other when the H_2O/CO ratio is 1:1. Similarly, the mole fractions of H_2 and CO_2 are the same. However, the mole fraction of CO is lower than that of H_2O under 710 °C. Similarly, the mole fraction of H_2 is less than that of CO_2. This is attributed to the consumption of H_2 to form CH_4 and H_2O. A higher H_2O/CO ratio can extend the operating temperature of the WGS reaction to lower temperature. When the H_2O/CO ratio is increased to 2:1, the formation of CH_4 and H_2O occurs below 640 °C. Therefore, the WGS reaction should be carried out at temperatures higher than 710 °C and 640 °C with H_2O/CO ratios of 1:1 and 2:1, respectively.

3.2. Experimental conversion

The CO conversion was measured under three situations: (1) blank reference, (2) with Ni catalyst, and (3) with Ni catalyst and *in situ* H_2 removal. In the first two situations, two different gas compositions were applied: 3% CO + 3% H_2O or 3% CO + 6% H_2O, while maintaining a constant flow rate of 20 sccm balanced by Ar. Only 3% CO + 6% H_2O gas composition was applied in situation (3). For the blank reference, CO and H_2O were fed into an empty quartz reactor. For the WGS reaction with Ni catalyst, the tubular membrane was installed in the quartz reactor exposing the Ni in the porous support and the effluent on the permeate side was blocked. No sweep gas was used and no H_2 was removed. Therefore, the membrane only functioned as a catalyst in this situation with the reactant gas mix passing by the Ni catalyst in the support tube surface. For the WGS reaction with Ni catalyst and *in situ* H_2 removal, the permeated side was connected to a mass spectrometer, so that the permeated H_2 concentration could be analyzed.

The mole fractions of H_2, CO, H_2O and CO_2 under these three reactor configurations are shown in Figs. 3–5. These mole fractions do not include the Ar diluent. The CH_4 concentration was below detection limits and ignored here. For the blank reference, the mole fraction of H_2 is the same as that of CO_2 under both H_2O/CO ratios of 1:1 and 2:1 (Fig. 3). The mole fractions of CO and H_2O equal to each other for a 1:1 H_2O/CO ratio as well.

For WGS with the Ni catalyst (Fig. 4), the mole fractions of species are similar with the thermodynamic data shown in Fig. 2. The mole fractions of H_2 and CO_2 agree with each other at elevated temperature and there is similar deviation at low temperatures. This indicates the WGS reaction approaches thermodynamic equilibrium in the presence of the Ni catalyst in the tubular support.

The mole fractions in Fig. 5 are just for the species in the feed side effluent. The permeated H_2 is not included. It is important to point out that no Ar was observed in the permeated gas so the membrane was leak free. The H_2 and CO_2 mole fractions were significantly different comparing Figs. 4(b) and 5. Both were under the WGS with Ni and a H_2O/CO ratio of 2:1, but the data in Fig. 5 were achieved with *in situ* H_2 removal. The CO_2 mole fraction was higher in Fig. 5 and increased with increasing temperature due to the *in situ* removal of H_2 overcoming the inherent thermodynamic limitation at high temperature. In addition, while the H_2 mole fraction decreased with increasing temperature in Fig. 4(b), it was almost independent of temperature in Fig. 5.

CO conversion is a very important parameter in the WGS reaction and needs to be maximized in order to increase H_2 production. The CO conversion is defined as follows:

$$\text{CO conversion}\,(\%) = \frac{F_{CO_2}^{out}}{F_{CO}^{in}} \times 100\% \qquad (2)$$

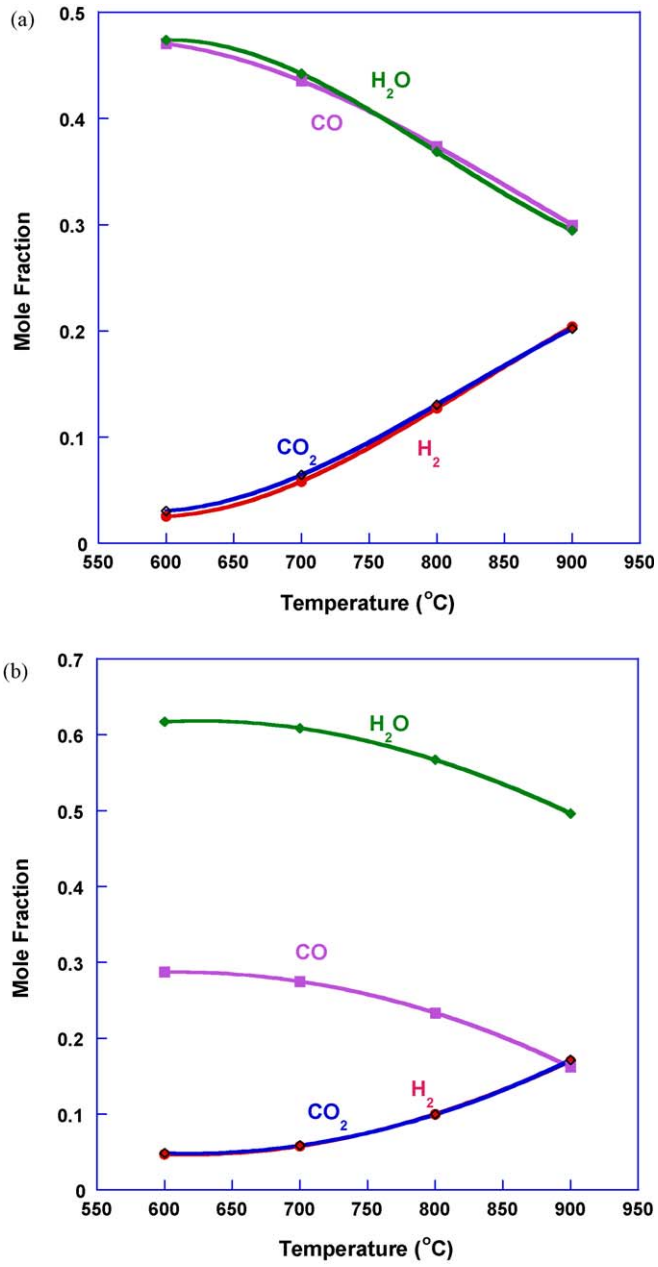

Fig. 3. Blank reference effluent gas composition as a function of temperature. (a) $H_2O/CO = 1:1$ and (b) $H_2O/CO = 2:1$

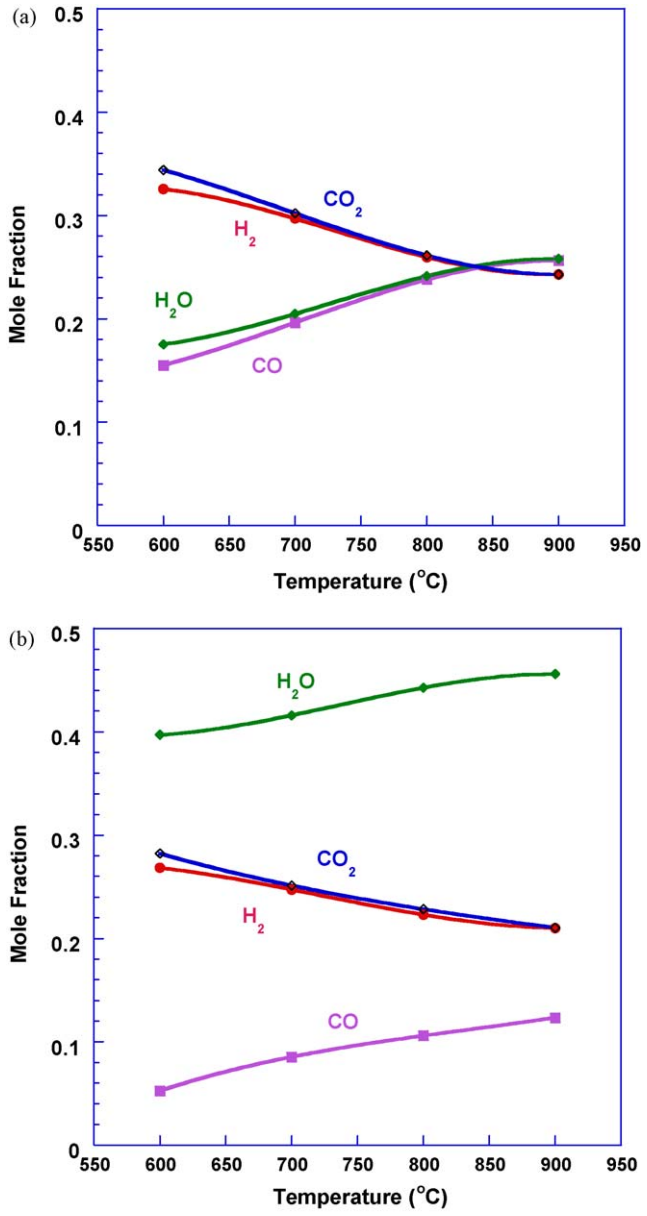

Fig. 4. Catalytic effluent gas composition as a function of temperature. $H_2O/CO = 1:1$ and (b) $H_2O/CO = 2:1$

where $F^{out}_{CO_2}$ and F^{in}_{CO} are CO_2 output flux and CO input flux, respectively.

Fig. 6 shows the CO conversion temperature dependence for different reactor configurations with a H_2O/CO ratio of 1:1 and 2:1, respectively and compares with their thermodynamic equilibrium data. The thermodynamic conversion decreases as the reaction temperature increases. This is consistent with the mole fraction decrease of H_2 and CO_2 as temperature increases in Fig. 2. At any temperature, the CO conversion under thermodynamic equilibrium increases with increasing H_2O/CO ratio from 1:1 to 2:1. A higher feed steam concentration moves the reaction (1) forward, resulting in higher CO conversion.

For the blank reference under both H_2O/CO ratios of 1:1 and 2:1, CO conversion was significantly lower than the thermodynamic values. The reaction rate increased with increasing temperature and the CO conversion approached theoretical at higher temperatures.

With the Ni catalyst, the CO conversion was comparable to and consistent with the thermodynamic values. The slight deviation, especially at lower temperatures, was attributed to side reactions which could take place during the WGS process [26].

According to the thermodynamic data, higher H_2O/CO ratio results in higher CO conversion. Therefore, the effect of *in situ* H_2 removal on the CO conversion was investigated under a H_2O/CO ratio of 2:1 (Fig. 6). Compared to the CO conversion with only the Ni catalyst, much higher CO conversion was achieved especially at high temperatures (46% increase at 900 °C). Since the permeated H_2 lowered the H_2 concentration in the product stream it moved the reaction further toward the product side resulting in higher CO conversion. Therefore, the H_2 membrane can help overcome the thermodynamic limitations and improve CO conversion. It simultaneously increases H_2 yield as well. This can also be applied to reduce the CO level in the H_2 gas produced from hydrocarbon fuels for proton-exchange membrane (PEM) fuel cells. The enhancement in CO conversion in WGS reaction with Pd based membrane reactors has also been reported [27,28]. A CO

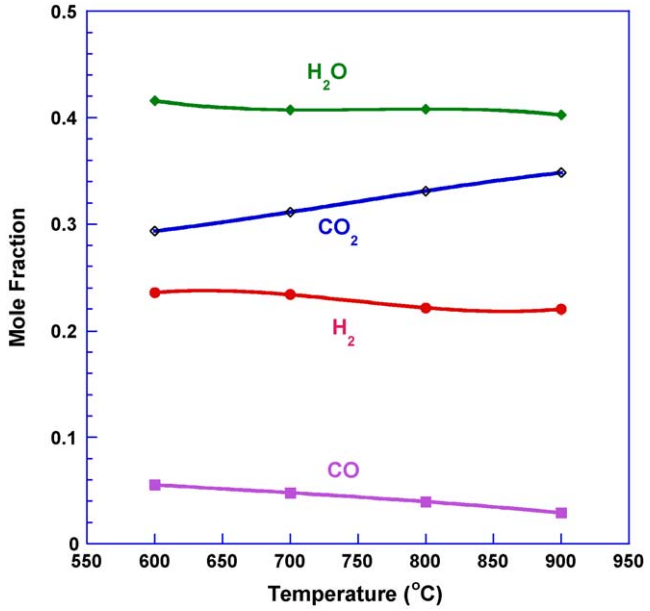

Fig. 5. Catalytic effluent gas composition with *in situ* H_2 removal as a function of temperature for a $H_2O/CO = 2:1$ feed gas.

conversion close to 100% was achieved at 325–330 °C compared to the equilibrium value, 80%, with Pd–Ag membranes [28]. The H_2 permeance through that 50 μm Pd–Ag membrane was 3.3×10^{-3} ml cm^2 min^{-1} Pa$^{-0.5}$ at 330 °C. However, the Palladium membranes are expensive, highly fragile, and their application is limited to low temperature, which limits thermal integration and leads to low kinetic reaction rates.

3.3. H_2 production

H_2 production for the blank reference increased with increasing temperature, in agreement with the CO conversion under the same

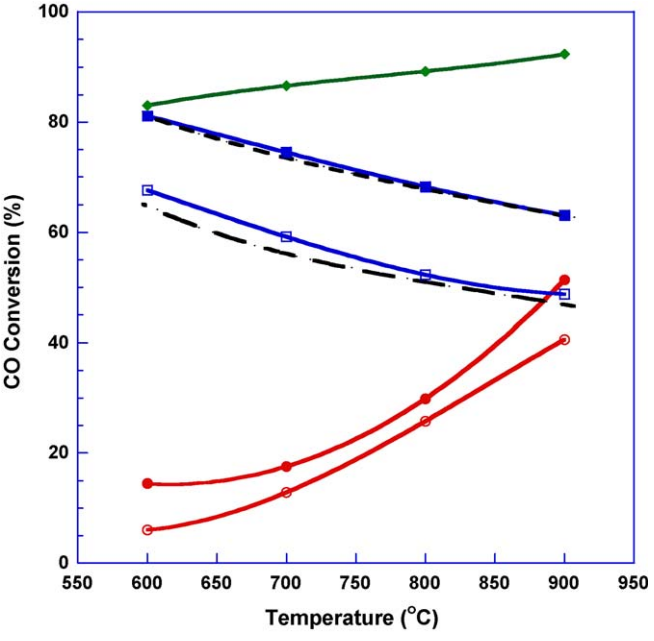

Fig. 6. Temperature dependence of CO conversion under 3% CO + 3% H_2O and 3% CO + 6% H_2O. ○ Blank reference ($H_2O/CO = 1:1$), ● blank reference ($H_2O/CO = 2:1$), – – thermodynamic data ($H_2O/CO = 1:1$), – thermodynamic data ($H_2O/CO = 2:1$), □ WGS with catalyst ($H_2O/CO = 1:1$), ■ WGS with catalyst ($H_2O/CO = 2:1$), ◆ WGS with catalyst and *in situ* H_2 removal ($H_2O/CO = 2:1$).

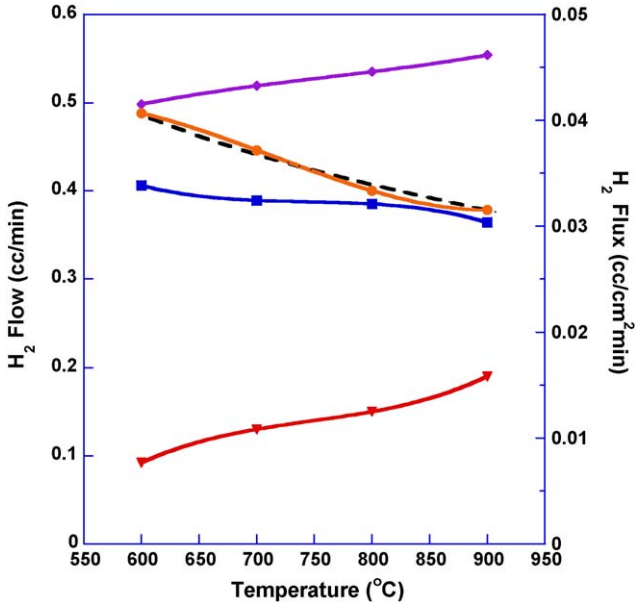

Fig. 7. H_2 production under 3% CO + 6% H_2O as a function of temperature for three reactor configurations. – Thermodynamic H_2 production, ● catalytic H_2 production without H_2 removal, ▼ pure permeated H_2 through membrane, ■ H_2 production in the feed side effluent with *in situ* H_2 removal, ◆ total catalytic H_2 production with *in situ* H_2 removal.

conditions as shown in Fig. 6. Fig. 7 shows the H_2 production with a H_2O/CO ratio of 2:1 as a function of temperature. The H_2 production with only the Ni catalyst decreased with increasing temperature consistent with the thermodynamic data due to the exothermic nature of the WGS reaction. The H_2 permeation flux increased with increasing temperature due to the higher ambipolar conductivity of $SrCe_{0.9}Eu_{0.1}O_{3-\delta}$ at elevated temperatures [22]. In addition, the H_2 production in the effluent gases from the feed side of the tube was essentially temperature independent with *in situ* H_2 removal. The total H_2 production with *in situ* H_2 removal is the sum of the H_2 in the feed side effluent and the permeated H_2. It increased with increasing temperature. The improvement was more significant at elevated temperatures

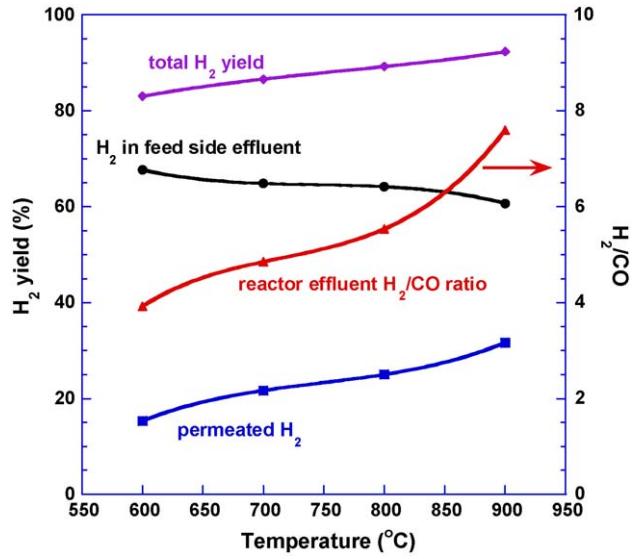

Fig. 8. H_2 yield and syngas H_2/CO ratio as a function of temperature under 3% CO + 6% H_2O and with *in situ* H_2 removal.

compared to the thermodynamic value. A 46% increase in total H_2 production was achieved at 900 °C.

The H_2 yield is defined:

$$H_2 \text{ yield}\,(\%) = \frac{F_{H_2}^{out}}{F_{CO}^{in}} \times 100\% \quad (3)$$

where $F_{H_2}^{out}$ and F_{CO}^{in} are the H_2 production and CO input flux, respectively.

The H_2 yield was plotted in Fig. 8 as well as the H_2/CO ratio in the feed side effluent with H_2 *in situ* removal and a H_2O/CO ratio of 2:1. The total H_2 yield is the sum of the permeated H_2 yield and the H_2 yield in the feed side effluent. The H_2 yield was in similar trend with the H_2 production (Fig. 7). The permeated H_2 yield and total H_2 yield were 32% and 92% at 900 °C, respectively. The feed side effluent consisted of H_2 and CO_2 rich gases together with the residual CO and H_2O. The H_2/CO ratio increased from 3.9 to 7.6 when the temperature increased from 700 to 900 °C.

Like other Cerates [11], the stability of $SrCe_{0.9}Eu_{0.1}O_{3-\delta}$ needs to be improved, especially under high CO_2 concentration and low temperature. The H_2 yield degrades at 1.8%/h under the WGS conditions and the stability improvement of this composition is discussed in our other work [29].

4. Conclusions

Water–gas shift reaction is constrained by thermodynamic equilibrium limitations. A tubular $SrCe_{0.9}Eu_{0.1}O_{3-\delta}$ hydrogen transport water–gas shift membrane reactor was fabricated. The CO conversion, H_2 production, H_2 yield and the H_2/CO ratio in the feed side effluent increase significantly with the WGS membrane. A 46% increase in CO conversion and total H_2 yield was achieved at 900 °C under 3% CO and 6% H_2O, resulting in a 92% single pass H_2 production yield and 32% single pass yield of pure permeated H_2. These results demonstrate the efficiency of hydrogen membrane reactors for the water–gas shift reaction.

Acknowledgments

This work was financially supported by NASA (NAG3-2930) and the Florida Institute for Sustainable Energy. Thanks to Sean Bishop for valuable discussion.

References

[1] Y. Li, Q. Fu, M. Flytzani-Stephanopoulos, Applied Catalysis B: Environmental 27 (3) (2000) 179.
[2] C. Rhodes, G.J. Hutchings, A.M. Ward, Catalysis Today 23 (1) (1995) 43.
[3] J. Pasel, R.C. Samsun, D. Schmitt, R. Peters, D. Stolten, Journal of Power Sources 152 (2005) 189.
[4] C.A. Udovich, Studies in Surface Science and Catalysis 119 (1998) 417.
[5] J.W. Phair, S.P.S. Badwal, Ionics 12 (2006) 103.
[6] S. Tosti, International Journal of Hydrogen Energy 28 (12) (2003) 1445.
[7] A.K. Garg, L.C.D. Jonghe, Journal of Material Science 28 (13) (1993) 3427.
[8] D. Lee, S.T. Oyama, Journal of Membrane Science 210 (2) (2002) 291.
[9] H. Iwahara, Solid State Ionics 86–88 (Part 1) (1996) 9.
[10] T. Schober, Solid State Ionics 162/163 (2003) 277.
[11] H. Matsumoto, T. Shimura, H. Iwahara, T. Higuchi, K. Yashiro, A. Kaimai, T. Kawada, J. Mizusaki, Journal of Alloys and Compounds 408–412 (2006) 456.
[12] T. Higuchi, T. Tsukamoto, H. Matsumoto, T. Shimura, K. Yashiro, T. Kawada, J. Mizusaki, S. Shin, T. Hattori, Solid State Ionics 176 (39/40) (2005) 2967.
[13] T. Tsuji, T. Nagano, Solid State Ionics 136/137 (2000) 179.
[14] X. Qi, Y.S. Lin, Solid State Ionics 120 (1999) 85.
[15] S. Hamakawa, L. Li, A. Li, E. Iglesia, Solid State Ionics 148 (1/2) (2002) 71.
[16] J. Guan, S.E. Dorris, U. Balachandran, L. Meilin, Solid State Ionics 110 (3/4) (1998) 303.
[17] S.J. Song, E.D. Wachsman, J. Rhodes, S.E. Dorris, U. Balachandran, Solid State Ionics 167 (1/2) (2004) 99.
[18] X. Qi, Y.S. Lin, Solid State Ionics 130 (1/2) (2000) 149.
[19] X. Wei, Y.S. Lin, Solid State Ionics 178 (35/36) (2008) 1804.
[20] H. Iwahara, T. Esaka, H. Uchida, N. Maeda, Solid State Ionics 3/4 (1981) 359.
[21] K.D. Kreuer, Solid State Ionics 125 (1–4) (1999) 285.
[22] T. Oh, H. Yoon, E.D. Wachsman, Solid State Ionics, in press.
[23] H. Yoon, T. Oh, J. Li, K. Duncan, E.D. Wachsman, Journal of the Electrochemical Society 156 (7) (2009) B791.
[24] H. Yoon, S. Song, T. Oh, J. Li, K. Duncan, E.D. Wachsman, Journal of the American Ceramic Society 92 (8) (2009) 1849.
[25] B. Sundman, B. Jansson, J.-O. Andersson, Calphad 9 (1985) 153.
[26] E. Xue, M. O'Keeffe, J.R.H. Ross, Catalysis Today 30 (1–3) (1996) 107.
[27] Y. Bi, H. Xu, W. Li, A. Goldbach, International Journal of Hydrogen Energy 34 (7) (2009) 2965.
[28] S. Tosti, A. Basile, G. Chiappetta, C. Rizzello, V. Violante, Chemical Engineering Journal 93 (1) (2003) 23.
[29] J. Li, H. Yoon, T. Oh, E.D. Wachsman, Journal of the Electrochemical Society, submitted for publication.